Applied Catalysis B: Environmental 154–155 (2014) 73–81

Contents lists available at ScienceDirect

Applied Catalysis B: Environmental

journal homepage: www.elsevier.com/locate/apcatb

# $FeO_x$-supported gold catalysts for catalytic removal of formaldehyde at room temperature

Bing-bing Chen[a,b], Xiao-bing Zhu[b], Mark Crocker[c], Yu Wang[a,b], Chuan Shi[a,b,*]

[a] Key Laboratory of Industrial Ecology and Environmental Engineering (MOE), Dalian University of Technology, Dalian, PR China
[b] Laboratory of Plasma Physical Chemistry, Dalian University of Technology, Dalian, PR China
[c] Center for Applied Energy Research, University of Kentucky, Lexington, KY 40511, USA

ARTICLE INFO

*Article history:*
Received 30 October 2013
Received in revised form 27 January 2014
Accepted 4 February 2014
Available online 14 February 2014

*Keywords:*
Formaldehyde
Catalytic oxidation
Gold
Iron oxide
Room temperature

ABSTRACT

$FeO_x$-supported Au catalysts prepared by co-precipitation (CP) were investigated for catalytic HCHO oxidation. The applied calcination temperature was found to greatly influence both the chemical properties and microstructure of the catalysts. Characterization using XRD, $H_2$-TPR and XPS suggested that lower calcination temperature improves the reducibility of the catalysts, and favors the presence of surface hydroxyl groups. Consequently, an $Au/FeO_x$ catalyst calcined at 200 °C afforded 100% conversion of HCHO into $CO_2$ and $H_2O$ at room temperature and under humid air. *In situ* DRIFTs studies suggested that the moisture was essential for deep oxidation of the formate intermediates into $CO_2$ and $H_2O$, this being the rate limiting step for catalytic HCHO oxidation.



## 1. Introduction

Gold was formerly believed to possess little activity as a heterogeneous catalyst due to its electronic configuration. The current interest in supported gold nanoparticles was initiated by Haruta et al. who first described the extraordinary activity of supported gold nanoparticles for low temperature oxidation of CO [1]. This finding has generated significant interest in gold catalysis. Apart from low temperature CO oxidation, gold catalysts have been shown to be active in many other reactions, such as the hydrogenation of carbon oxides, the water gas shift reaction (WGS), the preferential oxidation of CO in $H_2$-rich streams (PROX) and the oxidation of volatile organic compounds (VOCs) [2–4].

A variety of oxide-supported Au catalysts, such as $Au/Co_3O_4$–$CeO_2$, $Au/ZrO_2$, and $Au/CeO_2$, have been tested for HCHO catalytic oxidation [5–7]. Zhu et al. found that a mesoporous $ZrO_2$-supported gold catalyst completely oxidized HCHO at temperatures above 170 °C. It was suggested that HCHO molecules strongly adsorbed on the gold species and converted rapidly into formate species, which reacted with adsorbed oxygen on the surface of the gold to form the $CO_2$ product [8]. Zhang et al. successfully synthesized three-dimensionally ordered macroporous 3DOM $Au/CeO_2$ catalyst, which was found to exhibit superior catalytic activity as exemplified by 100% HCHO conversion at 75 °C. The unique structure of 3DOM $CeO_2$ favored high gold dispersions, which was believed to be a key factor in the enhancement of catalytic efficiency for HCHO oxidation [9]. Recently, Hao et al. reported that 50% HCHO conversion was achieved over a mesoporous $Au/Co_3O_4$ catalyst at room temperature. It was found that HCHO could be oxidized into formate by $Co^{3+}$, and it could be further transformed into bicarbonate or carbonate species, which then decomposed into $CO_2$ and $H_2O$ [10]. Moreover, in our previous study, 1% $Au/CeO_2$ catalyst prepared by deposition–precipitation with urea exhibited 100% conversion of HCHO into $CO_2$ and $H_2O$ at room temperature, even in the presence of water and at high GHSV (143,000 $h^{-1}$). Charge transfer from Au to $CeO_2$ weakened the Ce–O bond, leading to the generation of active surface oxygen which in turn contributed to the superior activity of the $Au/CeO_2$ catalyst [11]. It is clear from the above studies that the contribution of the support material to the performance of supported gold catalysts should not be neglected.

Iron oxide is a potential catalyst support due to its reducibility, stability, and ability for electron transfer. Recently, Zhang and co-workers [12] synthesized a novel $Pt/FeO_x$ catalyst for CO oxidation and preferential oxidation of CO in $H_2$, which consists of only single Pt atoms uniformly dispersed on a $FeO_x$ support.

* Corresponding author at: Key Laboratory of Industrial Ecology and Environmental Engineering (MOE), Dalian University of Technology, Dalian, People's Republic of China. Tel.: +86 411 84986083; fax: +86 411 84986083.
*E-mail address:* chuanshi@dlut.edu.cn (C. Shi).

http://dx.doi.org/10.1016/j.apcatb.2014.02.009
0926-3373/

Fu et al. [13] also found that Fe played a key role in forming a highly active and stable Fe–O–Pt structure in the PROX reaction. Moreover, gold supported on iron oxide has been intensively studied in a variety of other applications, including the water gas shift reaction and the selective hydrogenation of α,β-unsaturated aldehydes and ketones to the corresponding alcohols [14,15]. Recently, Li and co-workers [16] demonstrated the complete oxidation of formaldehyde over 7.10 wt% gold/iron-oxide catalyst at 80 °C, the high activity of the catalyst being attributed to the high dispersion of the gold particles which can activate the oxygen of the iron oxide support.

Herein, we report our recent results on ferric oxide-supported Au catalysts for HCHO oxidation at room temperature. It was found that a catalyst prepared by co-precipitation and calcined at 200 °C showed the best catalytic activity, complete oxidation of HCHO into $CO_2$ and $H_2O$ being achieved at room temperature and in humid air. Moisture was found to be essential for complete oxidation of HCHO at room temperature over $Au/FeO_x$ catalysts. This is quite different from our previous study using $Au/CeO_2$ catalysts, which could completely convert HCHO into $CO_2$ and $H_2O$ at room temperature either in dry or humid air. Based on catalyst characterization and *in situ* DRIFTs studies presented herein, surface hydroxyls were found to be active for further oxidation of reaction intermediates (such as formates, etc.) into $CO_2$ and $H_2O$, which proved to be the rate limiting step for HCHO oxidation.

## 2. Experimental

### 2.1. Catalyst preparation

All chemicals used in this work were of analytical grade and were used without further purification. Catalysts were prepared according to a co-precipitation method [17]. Aqueous solutions of $HAuCl_4$ (0.024 mol $L^{-1}$) and $Fe(NO_3)_3$ (1 mol $L^{-1}$) were mixed and added dropwise into a $Na_2CO_3$ (1 mol $L^{-1}$) solution at 60 °C with vigorous stirring. The final pH was adjusted to around 8. After stirring and aging for 4 h, the resulting precipitate was filtered and washed with hot distilled water, then dried at 60 °C for 6 h and calcined at 200 °C (denoted as $Au/FeO_x$-C200), 300 °C ($Au/FeO_x$-C300) and 400 °C ($Au/FeO_x$-C400) for 4 h.

### 2.2. Catalyst characterization

The Au loadings in the catalysts were determined by inductively coupled plasma-atomic emission spectroscopy (ICP-AES, Optima 2000DV, USA).

BET surface area determinations were performed using a nitrogen adsorption apparatus (Micromeritics, Tristar 3000).

Powder X-ray diffraction (XRD) patterns were recorded on a D/MAX-2400 powder diffractometer using Cu Kα radiation (λ = 0.1542 nm) in a 2θ range of 30–80°.

Transmission electron microscopy (TEM) images of the catalysts were obtained on a JEOL JEM-2000EX microscope operated at 200 KV. 100 Au nanoparticles were analyzed in order to construct the particle size histograms.

Hydrogen temperature programmed reduction ($H_2$-TPR) measurements were performed on a Micromeritics AutoChem II 2920 chemisorption analyzer. 50 mg samples were loaded and pretreated under Ar at 120 °C for 1 h to remove adsorbed $CO_2$ and $H_2O$. After cooling to 30 °C and introducing the reducing gas (5% $H_2$/Ar) at a flow rate of 50 ml $min^{-1}$, the temperature was ramped to 700 °C at 10 °C $min^{-1}$.

The surface chemical states of the $Au/FeO_x$ catalysts were examined by X-ray photoelectron spectroscopy (XPS, ESCALAB250 Thermo VG, USA) using an Al Kα X-ray source (1486.6 eV) operated at 15 kV and 300 W. Binding energies were corrected for surface charging by referencing them to the energy of the C1s peak of the contaminant carbon at 284.6 eV. The spectra were processed in XPSPEAK 4.1 program. In the spectra, the background was approximated by a Shirley profile. Quantitative Analysis: 1) the XPSPEAK 4.1 peak fitting program was applied to fit the Au 4f and O 1s spectrum, respectively. The peak area would obtain from the data reports; 2) find out the atomic sensitivity factors (ASF) of every constituent from the handbook of X Ray Photoelectron Spectroscopy; 3) the surface atomic ratio could be calculated according the peak area and ASF.

Infrared spectra were recorded on a Bruker Tensor 27 instrument equipped with a MCT detector using the DRIFT technique. Scans were collected from 4000 to 1000 $cm^{-1}$ (128 scans, resolution of 4 $cm^{-1}$). In adsorption experiments, the catalyst was placed in a DRIFT cell equipped with $CaF_2$ windows and was pretreated in a $N_2$ flow at 200 °C for 1 h. Subsequently, the reactant gas mixture was introduced into the DRIFT cell at room temperature via separate mass flow controllers at a flow rate of 100 ml $min^{-1}$. After a specified amount of time the HCHO flow was switched off and replaced by various gas streams.

### 2.3. Catalytic activity measurement

Catalyst tests were performed in a continuous flow fixed-bed quartz microreactor at atmospheric pressure. 0.19 g catalyst (40–60 mesh) was sandwiched between quartz wool layers in the tube reactor. All the feed gases used in this work were of high-purity grade (99.99%). The gas flow rates were adjusted and controlled by mass flow controllers. Gaseous HCHO was generated by flowing $N_2$ over paraformaldehyde (99%, Aldrich) in a thermostated bath. The concentration of HCHO was controlled by adjusting the flow rate of $N_2$ and the temperature of the thermostated bath. Gaseous $H_2O$ was carried into the gas stream by passing $N_2$ through a bubbler in a water bath at room temperature. The amount of water, expressed as the relative humidity (RH) at 25 °C, was controlled by adjusting the flow rate of $N_2$, while keeping the total flow unchanged. The HCHO/$N_2$ and $H_2O$/$N_2$ streams were then mixed with the main gas stream of $O_2$/$N_2$, leading to a typical feed gas composition of 80 ppm HCHO and 21 vol. % oxygen, balanced by nitrogen with a relative humidity (RH) of 50% (25 °C). The total flow rate was 100 ml $min^{-1}$, corresponding to a gas hourly space velocity (GHSV) of 34,000 $h^{-1}$.

Concentrations of CO and $CO_2$ were measured online using an infrared absorption spectrometer (SICK-MAIHAK-S710, Germany). In this work, it was not possible to monitor the HCHO concentration directly by Fourier transform-infrared spectroscopy (FT-IR) due to the interfering effects of water. Therefore, HCHO was measured by converting it to $CO_2$ in a homemade HCHO-to-$CO_2$ converter (CuO–$MnO_2$/γ-$Al_2O_3$ catalyst) at 300 °C and determining the amount of $CO_2$ formed. Several previous reports have likewise pointed out that for the accurate determination of HCHO, the HCHO should first be oxidized to $CO_2$ [18,19].

The conversion of HCHO was calculated as follows: $HCHO\ conversion\ (\%) = \frac{[CO_2]_{out\,vol.\%}}{[HCHO]_{in\,vol.\%}} \times 100$,

Where $[CO_2]_{out}$ is the $CO_2$ concentration in the product gas stream (vol.%) and $[HCHO]_{in}$ is the HCHO concentration in the feed gas (vol.%). In all cases the carbon balance was near 100% [6].

Rate of HCHO oxidation has been determined at low conversion by assuming differential reactor conditions; accuracy of rate values is within 20%, as determined by repeated measurements at fixed temperature. Reaction conditions were chosen to minimize the effect of mass and heat transfer phenomena. The absence of external and internal diffusion limitation was confirmed by experiments (see Fig. S4).

**Table 1**
Physicochemical property of $FeO_x$ and $Au/FeO_x$ catalysts.

| Sample | Au content (wt%) | | $S_{BET}$ ($m^2\ g^{-1}$) |
|---|---|---|---|
| | Nominal | Actual | |
| $FeO_x$-C200 | – | – | 217.8 |
| $Au/FeO_x$-C200 | 1 | 0.69 | 186.9 |
| $Au/FeO_x$-C300 | 1 | 0.82 | 97.8 |
| $Au/FeO_x$-C400 | 1 | 0.84 | 37.7 |

## 3. Results

### 3.1. Physicochemical properties of $Au/FeO_x$ catalysts

Physiochemical properties of the $Au/FeO_x$ catalysts are summarized in Table 1. It is noticeable that the Au contents measured by ICP increased with increasing calcination temperature, while catalyst BET surface areas decreased greatly. This increase in Au content is likely to be related to the loss of surface OH groups, carbonates/nitrates, and adsorbed water on the support [20], which is confirmed by FT-IR measurements discussed below.

XRD patterns of the $Au/FeO_x$ catalysts calcined at different temperatures are shown in Fig. 1. There was no detectable formation of crystalline ferric oxide in the $Au/FeO_x$-C200 sample; instead, $Au/FeO_x$-C200 showed very weak and broad diffraction lines at $2\theta = 35.89$, 40.79 and 61.34°, which can be indexed as a reflection of ferrihydrite ($Fe_5HO_8{\cdot}4H_2O$) or hematite ($\alpha$-$Fe_2O_3$). Due to the rather similar diffraction positions, it is not possible to distinguish between $Fe_5HO_8{\cdot}4H_2O$ and $\alpha$-$Fe_2O_3$. According to the results of Hutchings et al. [21] and Daniells et al. [22], $Au/FeO_x$ prepared by the CP method with calcination below 300 °C was mainly composed of $\alpha$-$Fe_2O_3$ and $Fe_5HO_8{\cdot}4H_2O$. This suggests that ferrihydrite and hematite may co-exist in the $Au/FeO_x$-C200 sample [21–23]. A crystalline hematite phase evolved as a result of increased calcination temperature, which is associated with the decrease of surface area to 97.8 and 37.7 $m^2\ g^{-1}$ for the samples calcined at 300 and 400 °C, respectively [24]. No gold species could be detected by XRD for any of the $Au/FeO_x$ samples, indicating that the gold is highly dispersed on the support.

The $H_2$-TPR profiles of the $Au/FeO_x$ catalysts calcined at different temperatures are presented in Fig. 2. To obtain a better understanding of the TPR profiles of the $Au/FeO_x$ samples, $FeO_x$ samples

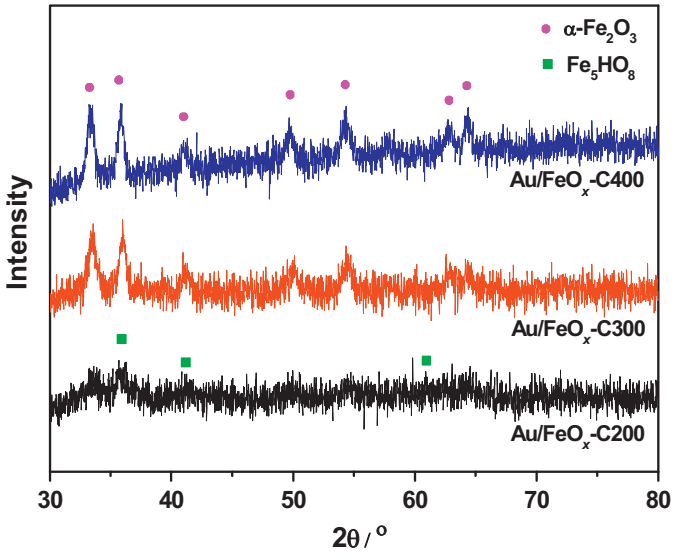


**Fig. 1.** XRD patterns of 1 wt% $Au/FeO_x$ catalysts calcined at different temperatures.

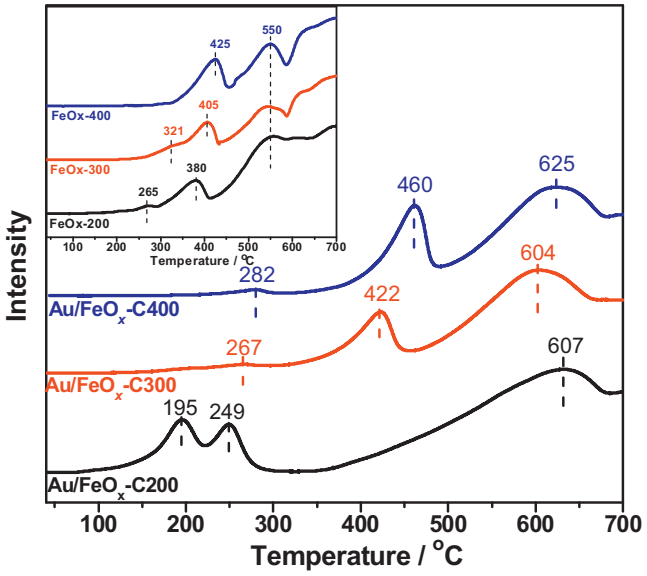


**Fig. 2.** $H_2$-TPR profiles of $FeO_x$ and 1 wt% $Au/FeO_x$ catalysts calcined at different temperatures.

were also measured as references (shown in the inset of Fig. 2). For the $FeO_x$-200 sample, three reduction peaks were present at 265, 380 and 550 °C. Based on previous studies [25–27], the peak at 265 °C can be attributed to the reduction of surface oxygen and hydroxyl species, the peak at 380 °C corresponded to the reduction of $Fe_2O_3$ to $Fe_3O_4$, and the high temperature reduction peak at 550 °C represented the transition of $Fe_3O_4$ to FeO. The intensity of the first reduction peak decreased as the calcination temperature increased, implying the loss of surface oxygen and OH groups. Simultaneously, the reduction temperature for surface oxygen and hydroxyl species shifted to higher values, as did the temperature of the $Fe_2O_3$ to $Fe_3O_4$ transition, although the reduction temperature of $Fe_3O_4$ to FeO remained unchanged. It is known that the reduction temperature from $Fe_2O_3$ to $Fe_3O_4$ can be influenced by the surface of the material (an increase in surface area causes a shift to lower reduction temperature) [25].

Compared with the TPR behavior of the $FeO_x$-200 reference, the addition of gold dramatically modified the reduction features of the $Au/FeO_x$-C200 sample. Specifically, the first two reduction peaks shifted to much lower temperatures (to ~195 and 249 °C, respectively). Such enhanced reduction of the support may be due to increasing the lattice defect and the surface oxygen vacancy of the $FeO_x$ support caused by the presence of Au [26], this phenomenon being found to be most prominent over the catalyst with the lowest calcination temperature. With increasing calcination temperature, the Au–O–Fe interaction became much weaker as indicated by the similar reduction behavior of the support before and after Au addition.

XPS analysis was carried out on the $Au/FeO_x$ samples, the results being shown in Fig. 3. The Au 4f core level spectra of the catalyst were deconvoluted into several components, the results being listed in Table 2. For all of the $Au/FeO_x$ catalysts the Au $4f_{5/2}$ peak was centered at ~84.0 eV, which is very closed to binding energy of metallic Au and which indicates that the gold species on the catalyst surface were metallic in nature [11,29].

XPS spectra corresponding to the O 1s region of the $Au/FeO_x$ samples are shown in Fig. 3B. By means of deconvolution, the distribution of oxygen species was estimated and is reported in Table 2. Two kinds of oxygen species are evident, one with an O 1s binding energy in the range of 531.2–530.6 eV which is assigned to surface adsorbed oxygen and hydroxyl species, while that in the range of

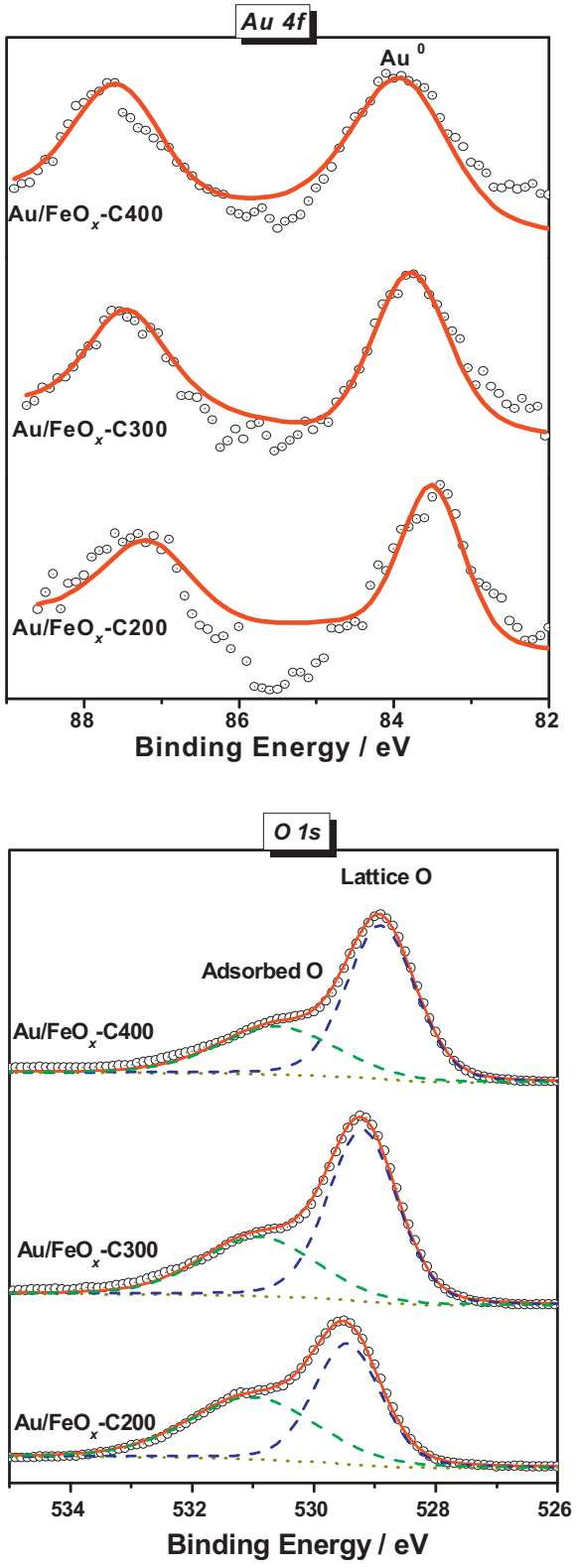


**Fig. 3.** (A) XPS spectra showing the Au 4f region for the $Au/FeO_x$ catalysts calcined at different temperatures (B) XPS spectra showing the O 1s region for the $Au/FeO_x$ catalysts calcined at different temperatures.

529.6–528.9 eV is ascribed to lattice oxygen [28]. Compared with the other $Au/FeO_x$ samples, $Au/FeO_x$-C200 is significantly enriched with surface oxygen and hydroxyl species, this finding being in agreement with the results of $H_2$-TPR.

**Table 2**
XPS analysis of $Au/FeO_x$ catalysts calcined at different temperatures.

| Catalyst | Peak position (eV) | | | $Au^0$ (at.%) | $(O_{ads}+OH)/O_{latt}$ |
|---|---|---|---|---|---|
| | $Au^0$ | $O_{latt}$ | $O_{ads}+OH$ | | |
| $Au/FeO_x$-C200 | 83.5 | 529.5 | 531 | 0.003 | 0.974 |
| $Au/FeO_x$-C300 | 83.8 | 529.2 | 530.9 | 0.006 | 0.564 |
| $Au/FeO_x$-C400 | 83.9 | 528.9 | 530.6 | 0.016 | 0.528 |

TEM observations of $Au/FeO_x$-C200 and $Au/FeO_x$-C400 are shown in Fig. 4. In the case of the $Au/FeO_x$-C200 catalyst, the Au species were highly dispersed and the average particle size was 3–4 nm (the average particle size was obtained from the TEM measurement of 100 Au-NPs, the more TEM images were shown in the Fig. S1). Furthermore, the supports appeared uniform and amorphous in nature, which agrees with the XRD results discussed above. In contrast, TEM images of the sample calcined at 400 °C showed the presence of discrete metallic Au nanoparticles with typical diameters of 5–7 nm. Notably, the support was transformed into highly crystalline $\alpha$-$Fe_2O_3$ grains which were typically about 30 nm in size. This observation correlates well with the measured drop of surface area from 187 $m^2\,g^{-1}$ in $Au/FeO_x$-C200 to 38 $m^2\,g^{-1}$ for the 400 °C calcined sample [24].

Fig. 5 displays the FT-IR spectra of $Au/FeO_x$ catalysts calcined at different temperatures. The $Au/FeO_x$-C200 catalyst exhibited a broad, strong absorbance at 3000–3680 $cm^{-1}$, this being attributed to the stretching vibration of OH groups and adsorbed water on the $FeO_x$ support. In addition, three intense bands in the 1200–1700 $cm^{-1}$ region were observed. The band centered at ~1640 $cm^{-1}$ can be assigned to the deformation vibration of $H_2O$ while the other two intense bands centered at 1496 and 1373 $cm^{-1}$ may be due to the superposition of carbonate and nitrate species on the $FeO_x$ support. Calcination at 300 °C or above resulted in the removal of physisorbed water and dehydroxylation, as well as in the decomposition of carbonate and nitrate species on the $FeO_x$ support, as indicated by the significant decrease in the intensities of the related absorbance bands [20,24].

### 3.2. Catalytic activity

The $Au/FeO_x$ catalysts were evaluated for HCHO oxidation at room temperature (RT), as shown in Fig. 6. The $Au/FeO_x$-C200 catalyst exhibited the highest activity, with reaction rate of 10.78 $\mu mol\,s^{-1}\,g(Au)^{-1}$ at RT. Indeed, this appears to be the highest reaction rate of HCHO oxidation at room temperature reported over $Au/FeO_x$ catalysts, as summarized and compared in Table S1 [16]. With increase of the calcination temperature from 200 to 400 °C, the reaction rate was decreased greatly, it was 2.16 $\mu mol\,s^{-1}\,g(Au)^{-1}$ over $Au/FeO_x$-C400 catalyst. This result clearly demonstrates that the use of elevated calcination temperatures has a negative effect on the catalytic performance of $Au/FeO_x$ samples in HCHO oxidation. The mean Au particle sizes, reaction rate and TOF of $Au/FeO_x$-C200 and $Au/FeO_x$-C400 catalysts were listed in Table 1. It was observed that, within the experimental error, the turnover frequency of HCHO conversion was closely depend on the Au particle size. However, it is noted that the morphology and chemical properties of $FeO_x$ itself were also changed with elevated calcination temperatures. Therefore, it was hard to distinguish the change of TOF was caused by a variation in Au particle size or an effect of support due to their strong interactions. Further investigations were needed to clarify it.

Fig. 7A shows the Arrhenius plots over $Au/FeO_x$-C200 catalyst in dry air and humid air conditions with different relative humidity at HCHO conversion <20% (at which the reaction temperature range was 25–35 °C). The data of apparent activation energies ($E_a$) were

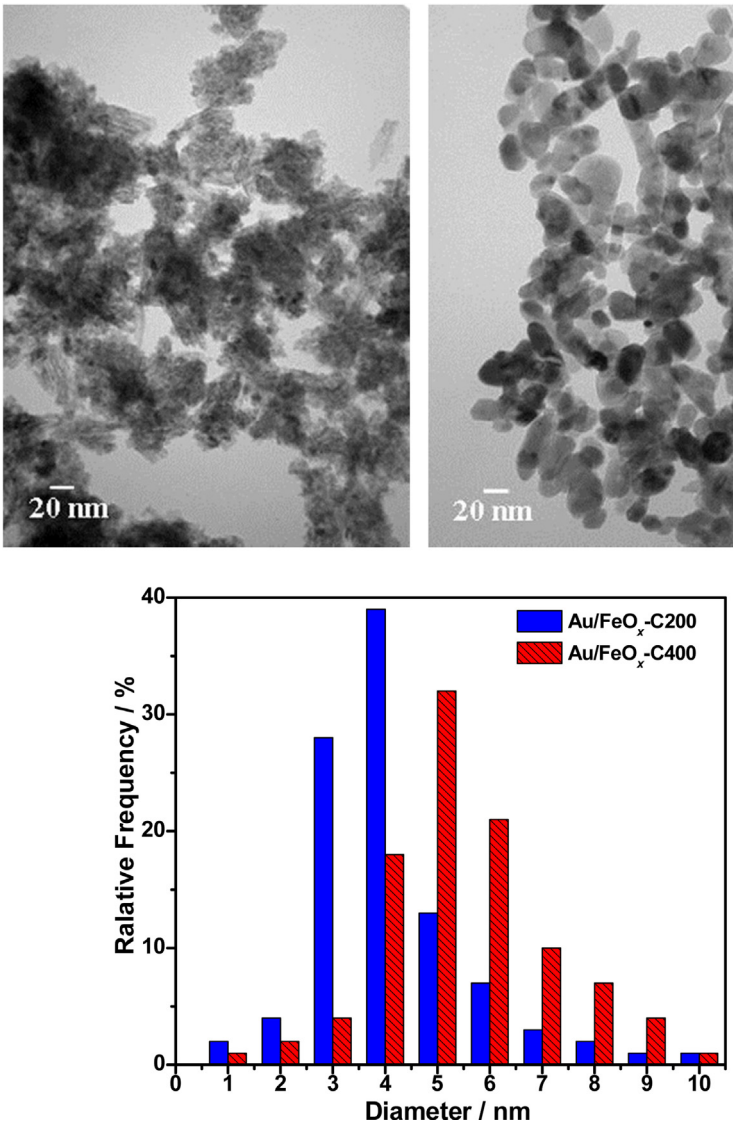


**Fig. 4.** TEM images of Au/FeO$_x$-C200 (top left) and Au/FeO$_x$-C400 (top right) catalysts and corresponding Au particle size distributions.

determined from the slopes of the fitted lines and summarized in Table 4. It can be clearly seen that the apparent activation energy ($E_a$) of Au/FeO$_x$-C200 catalyst was 172.1 kJ/mol in the dry gas condition, which was much higher than those (51.79–56.95 kJ/mol) in humid gas conditions. It suggests that presence of humidity might provide another reaction pathway with much lower $E_a$ values for HCHO oxidation (it will be discussed in the following section). When the relative humidity was increased to 50%, the catalyst exhibited the lowest $E_a$ value (51.79 kJ/mol). In contrast, it is worth noting that upon further increase of the relative humidity to 75%, the $E_a$ value of HCHO oxidation increased to 55.84 kJ/mol, demonstrating that addition of a certain amount of water enhances the activity of the Au/FeO$_x$ catalyst (RH ≤ 50%), while further increase in the moisture content inhibits the catalytic activity. However, the $E_a$ values were in the same level in humid air conditions compared with that in dry air, suggesting that the reaction mechanism was not changed with variation of RH.

A durability test on the Au/FeO$_x$-C200 catalyst was conducted under conditions corresponding to 80 ppm initial HCHO concentration, 50% relative humidity, and 68,200 h$^{-1}$ GHSV. As shown in Fig. 7B, no deactivation could be observed after operation for 1800 min, and the formation of CO was never detected, i.e., the HCHO conversion was 74%, indicating that the 1 wt% Au/FeO$_x$-C200 catalyst is quite stable under these conditions.

**Table 3**
Comparison of the reactivity of HCHO oxidation over Au/FeO$_x$ catalyst with different calcination temperature.

| Catalyst | $d_{Au}$[a] (nm) | Conv. (%)[b] | Reaction rate (μmol s$^{-1}$ g(Au)$^{-1}$)[b] | TOF × 10$^{-3}$ (s$^{-1}$)[b] |
|---|---|---|---|---|
| Au/FeO$_x$-C200 | 3.5 | 11.9 | 10.78 | 7.43 |
| Au/FeO$_x$-C400 | 5.8 | 11.9 | 2.16 | 2.47 |

[a] Average gold particle size estimated by statistic analysis from TEM results.
[b] Reaction condition: Au/FeO$_x$-C200: 0.01 g catalyst diluted with 0.12 g SiO$_2$; Au/FeO$_x$-C400: 0.05 g catalyst diluted with 0.08 g SiO$_2$, keeping the GHSV = 68,200 h$^{-1}$, 80 ppm HCHO/21%O$_2$/N$_2$, RH = 50%(25 °C).

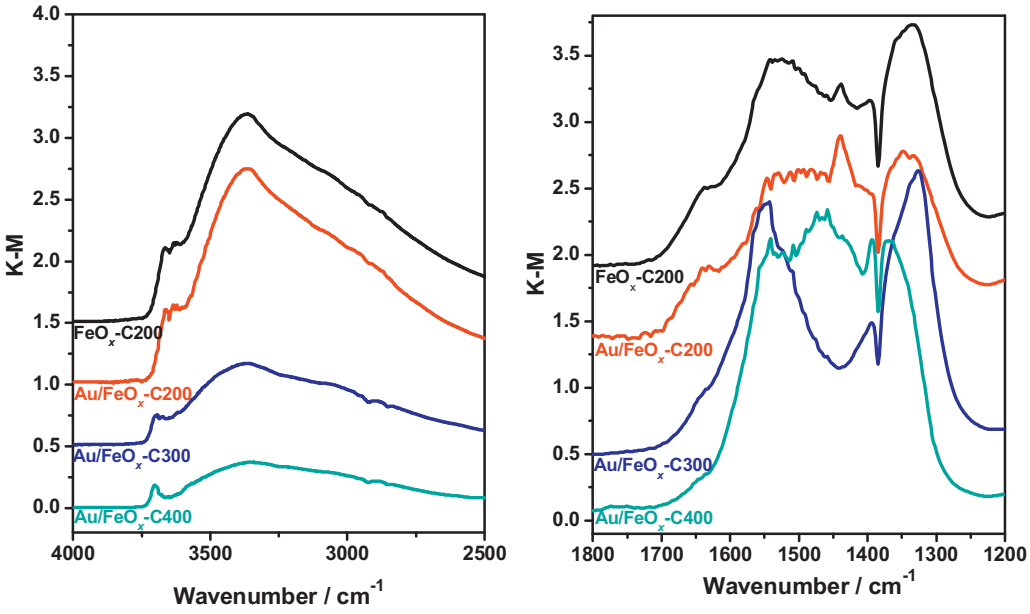


**Fig. 5.** FT-IR spectra of $FeO_x$ and $Au/FeO_x$ catalysts.

### 3.3. *In situ* DRIFTs study

*In situ* DRIFT spectra of the $Au/FeO_x$-C200 catalyst, obtained upon exposure to different gas streams at room temperature, are shown in Fig. 8. Upon exposure to 80 ppm $HCHO/N_2$, bands were observed at 2864, 2805, 1620 and 1102 $cm^{-1}$. According to the literature, the bands at 2864 and 2805 $cm^{-1}$ can be attributed to the $\nu$(C–H) stretch of formate and polyoxymethylene (POM) species, the band at 1620 $cm^{-1}$ is due to the asymmetric $\nu_{as}$(COO) stretch of formate species and the band at 1102 $cm^{-1}$ is due to the $\nu$(CO) stretch of POM [30,31]. No peaks associated with formaldehyde were detected, consistent with immediate oxidation of the HCHO after its adsorption without participation of gaseous $O_2$. Upon introducing $O_2$ into HCHO-containing feed stream, the intensity of band at 1620 $cm^{-1}$ became relative stronger, which had been assigned to the asymmetric $\nu_{as}$(COO) stretch of formate species. The other bands attributed to the formate and POM species were also observed. When the catalyst was exposed to feed gas

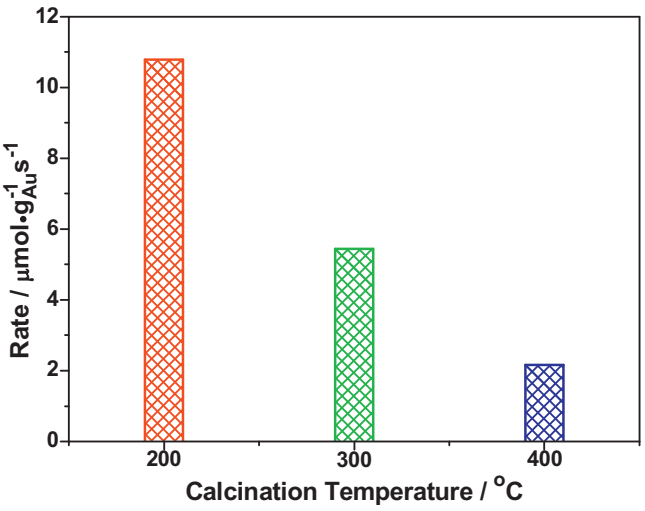


**Fig. 6.** The effect of calcination temperature on reaction rate of HCHO oxidation over the $Au/FeO_x$ catalysts. Reaction conditions: 80 ppm $HCHO/21\%O_2/N_2$, RH = 50% (25 °C ), RT, GHSV = 68,200 $h^{-1}$.

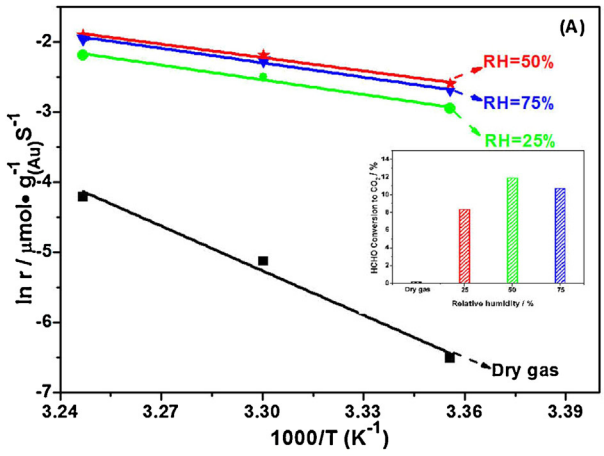


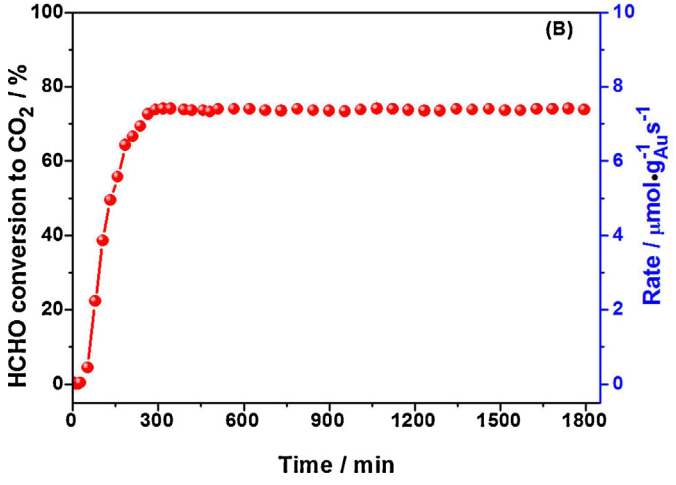


**Fig. 7.** (A) Arrhenius plots of reaction rates for oxidation of HCHO over the $Au/FeO_x$-C200 catalyst at different relative humidity; (B) Durability test on the $Au/FeO_x$ catalyst for HCHO oxidation. Reaction conditions: 80 ppm $HCHO/21\%$ $O_2/N_2$, RH = 50% (25 °C) GHSV = 68,200 $h^{-1}$.

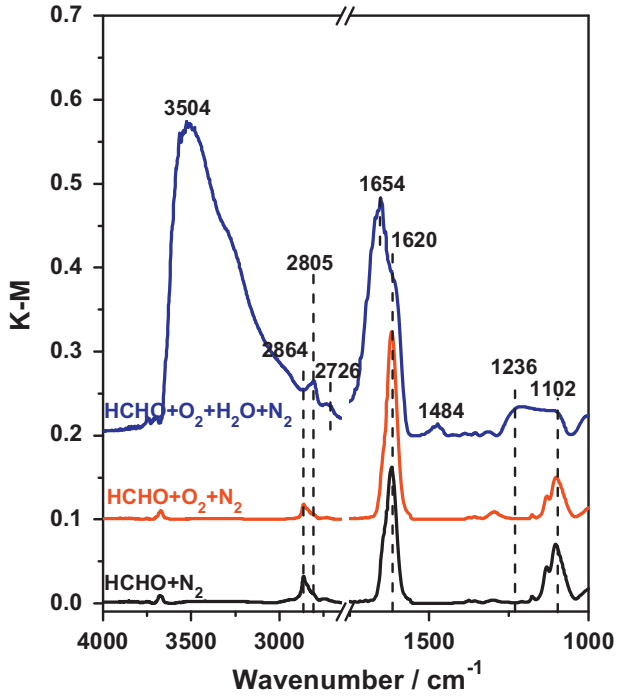


**Fig. 8.** *In situ* DRIFT spectra of HCHO adsorption on 1 wt% Au/$FeO_x$ after 90 min under various atmospheres at RT.

containing HCHO, $H_2O$ and $O_2$, besides new bands at 1654 $cm^{-1}$ due to adsorbed water [$\delta$(H–O–H)] and at 3504 $cm^{-1}$ due to isolated hydroxyl groups [$\nu$(OH)] strongly perturbed by hydrogen bonding, bands appeared at 1484 and 1236 $cm^{-1}$ ascribed to dioxymethylene (DOM). This observation is consistent with partial oxidation of HCHO directly to DOM species and/or transformation of POM into DOM, which could further combine with surface oxygen into formate species [32]. Relative to the case without water present, the bands attributed to formate species were stronger. Comparing the reaction intermediates formed over the Au/$FeO_x$-C200 catalyst upon exposure to the different HCHO-containing streams, it is clear that formate species formed even in the absence of $O_2$ and $H_2O$, suggesting that the surface oxygen or OH groups of the catalyst are active in the partial oxidation of HCHO into $[HCOO]_s$. The presence of gas phase oxygen enhanced the formation of formate species, while the presence of water did not appear to inhibit the formate formation [11,19].

The disappearance of the formates upon exposure to dry and wet gas streams is compared in Fig. 9. Samples were first exposed to 80 ppm HCHO/21%$O_2$/$N_2$ (for Fig. 9A) and 80 ppm HCHO/21%$O_2$/$H_2O$ (RH = 50%)/$N_2$ (For Fig. 9B) at room temperature for 150 min. After that, it was switched to dry air or humid air (without HCHO containing) to study the oxidation of the formate species with elevated temperatures. As shown in Fig. 9A, no obvious decrease in the intensities of the bands due to the formates was observed upon exposure to the dry gas for 60 min in the temperature range from 25 to 80 °C. However, upon heating to 100 °C, the intensities of the bands at 1620 $cm^{-1}$ decreased slightly, and complete oxidation of formate species occurred at 150 °C over the Au/$FeO_x$-C200 catalyst. In contrast, the formate band intensity (1620 $cm^{-1}$) decreased gradually in the presence of water, even at room temperature. A fast decrease in band intensity was observed during the first 1 h, while on standing at 25 °C for 6 h, the band attributed to formate species nearly completely disappeared. However, the intensity of the bands at 1484, 1236 and 1102 $cm^{-1}$ decreased slowly, which may be due to the incomplete oxidation of formate into carbonates [33], which gave the same positions with those of DOM and POM. The consumption of the formate intermediates over Au/$FeO_x$-C300 and Au/$FeO_x$-C400 catalysts were also investigated using *in situ* DRIFTs as shown in Fig. S3. After the switch to wet air without HCHO, partial consumption of the formates was observed at room temperature. Upon increasing temperature to 120 and 150 °C, the bands ascribed to formate species could be completely oxidized over Au/$FeO_x$-C300 and Au/$FeO_x$-C400 catalysts, respectively.

## 4. Discussion

Due to their reducibility and ability to stabilize supported noble metals, iron oxides have recently attracted much attention as catalyst supports. Indeed, they are reported to disperse single Pt atoms for both CO oxidation and PROX [12]. Benefitting from strong interactions between the support and the metal, Pt/$FeO_x$ has been demonstrated to possess superior activity in PROX [13]. In the case of HCHO oxidation, while Pt/$Fe_2O_3$ exhibited high activity, achieving complete oxidation of HCHO at room temperature [34], $FeO_x$-supported gold catalysts were found to be less active. The catalyst containing 7.10 wt% of gold exhibited the highest catalytic activity, which could be completely oxidized HCHO into $CO_2$ and $H_2O$ at 80 °C (6.25 mg/$m^3$ HCHO/air, GHSV = 54,000 $h^{-1}$ ml/g) [16].

In the present paper, 1 wt% Au/$FeO_x$ catalysts were prepared by the co-precipitation method. It was found that the calcination temperature applied exerts a significant influence on the chemical composition and microstructure of the catalysts. Lower calcination temperature enhances the reducibility of the catalyst, and favors an abundance of surface hydroxyls. As a consequence of the above characteristics, Au/$FeO_x$ was found to be highly active for HCHO oxidation at room temperature and in humid air. In the following section, the effects of these two factors on the microstructure and catalytic behavior of Au/$FeO_x$ catalysts are discussed.

$N_2$ physisorption results showed that the Au/$FeO_x$-C200 catalyst had the largest specific surface area, the surface area decreasing sharply with increasing calcination temperature. The calcination temperature also influenced the composition of the catalyst. The Au/$FeO_x$-C200 catalyst consisted of amorphous ferrihydrite and hematite, and was rich in surface hydroxyl groups. However, the amorphous phase transformed gradually into crystalline $\alpha$-$Fe_2O_3$ when it was calcined at or above 300 °C. Upon increasing the calcination temperature to 400 °C, the morphology of the support transformed from amorphous to well-crystallized $\alpha$-$Fe_2O_3$ with a particle size of ca. 30 nm. The similar phenomenon was observed on gold/iron oxide system, which had been reported by Minico et al. [36]. Accompanying this phase transformation, there was a loss of surface hydroxyls as indicated by FTIR. In addition, TEM results clearly showed the growth tendency of gold particles with increase of calcination temperature. Consequently, the mean Au particle size of Au/$FeO_x$-C200 (3–4 nm) was smaller than that of Au/$FeO_x$-C400 (5–7 nm).

After loading with Au, the redox properties of the $FeO_x$ support were greatly modified, especially for the Au/$FeO_x$-C200 sample. Specifically, the $FeO_x$ reduction peaks shifted to much lower temperature after loading with Au, although this was not the case for the samples calcined at higher temperatures. In fact, strong metal-support interactions have long been recognized [35]. Gold nanoparticles dispersed on the support are suggested to increase the in lattice defect and the surface oxygen vacancies, leading to generates the active surface oxygen species and facilitates reduction of the oxides at lower temperatures [23]. Indeed, evidence for the surface oxygen and OH groups is provided in this work by XPS measurements (Fig. 3), a higher ratio of $O_{ads}/O_{latt}$ being present in the Au/$FeO_x$-C200 catalyst compared to the other samples. These oxygen species could be reduced at low temperatures as evidenced by $H_2$-TPR (Fig. 2), which contributes to the superior activity of the

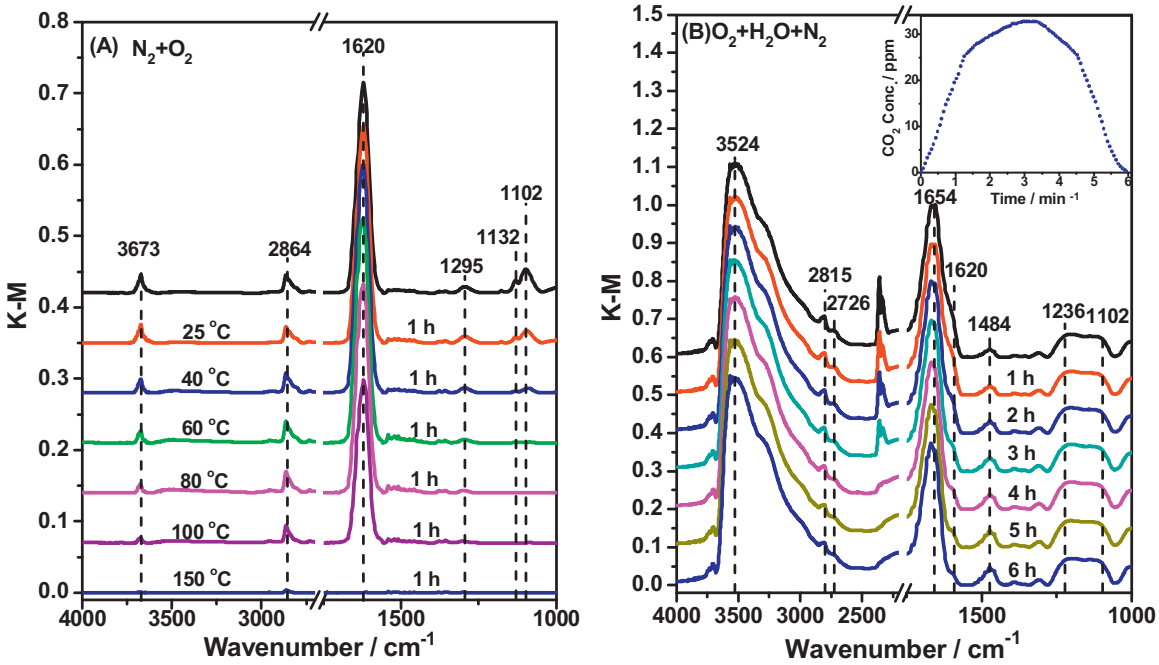


**Fig. 9.** (A) *In situ* DRIFT spectra of formate consumption over Au/$FeO_x$-C200 in dry air following exposure to 80 ppm HCHO/21%$O_2$/$N_2$ for 150 min; (B) *In situ* DRIFT spectra of formate consumption over Au/$FeO_x$-C200 in wet air following exposure to 80 ppm HCHO/21%$O_2$/$H_2O$ (RH = 50%)/$N_2$ for 150 min.

Au/$FeO_x$-C200 catalyst for catalytic HCHO oxidation. With increasing calcination temperature, there is loss of surface area and surface hydroxyl groups, which results in an increase in gold particle size and changes in the microstructure of the support. The larger gold particle size (TEM images) (as shown in Table 3), the lower ratio of $O_{ads}/O_{latt}$ (XPS measurements) and higher reduction temperatures for surface oxygen and hydroxyl species ($H_2$-TPR measurements), in turn, leads to the lower reaction rate for HCHO oxidation over Au/$FeO_x$-C300 and Au/$FeO_x$-C400 catalysts as shown in Fig. 6.

The effect of moisture on the formation and consumption of reaction intermediates was investigated over Au/$FeO_x$-C200 catalyst using *in situ* DRIFTs. First, the influence of $O_2$ and $O_2/H_2O$ on the formation of the intermediates was studied as shown in Fig. 8. It is apparent that HCHO was rapidly oxidized into formate species in the absence of $O_2$, suggesting that the adsorbed HCHO could be oxidized to formate by the surface oxygen and hydroxyl groups of the catalyst, as indicated by Eqs. (1) and (2). The intensity of the formate IR bands was found to increase upon exposure of the catalyst to HCHO–$O_2$ and HCHO–$O_2$–$H_2O$ mixtures, indicating that gaseous oxygen replenishes the oxygen vacancies by dissociation on the catalyst surface, thereby producing more surface oxygen and consequently additional formate species.

$$[HCHO]_s + [O]_s \rightarrow [HCOO]_s + [H]_s \quad (1)$$

$$[HCHO]_s + [OH]_s \rightarrow [HCOO]_s + 2[H]_s \quad (2)$$

In addition, in our previous study [11], the time required for formate formation exactly coincided with the time length of the induction period for the HCHO oxidation over the Au/$CeO_2$ catalyst as evidenced by *in situ* DRIFTs. Therefore, it is reasonable to deduce that the long induction period for oxidation of HCHO over Au/$FeO_x$-C200 catalyst in Fig. 7B correlated with the formate formation.

DRIFTs results also provide insights into the effects of moisture and temperature on the consumption of the formate intermediates. As shown in Fig. 9, there was no consumption of the formates at room temperature or indeed below 80 °C over Au/$FeO_x$-C200 in dry air. Upon increasing the temperature to 100 °C, the bands ascribed to the formate species decreased slightly, implying the beginning of their oxidation. At 150 °C, the formate species were completely oxidized. In contrast, the consumption of the formate species occurred at room temperature in the presence of moisture. Significantly, the temperature required for complete formate consumption is consistent with reaction rate of the HCHO oxidation shown in Fig. 7(A). Complete consumption of the formates was observed at 150 °C in dry air, while at the same temperature, 100% HCHO conversion was achieved in microreactor tests. In comparison, Au/$FeO_x$-C200 was active at room temperature for HCHO oxidation in humid air, while the consumption of formates was observed at room temperature by DRIFTs. These results indicate that the oxidation of the surface formates was the rate limiting step over the Au/$FeO_x$ catalysts.

As noted above, formate formation was fast and took place on the support even without the presence of gaseous $O_2$ (Fig. S1), the

**Table 4**
Apparent activation energies ($E_a$) and Turnover frequencies (TOFs) for Au/$FeO_x$-C200 catalyst evaluated in various relative humidity.

| Relative humidity | $d_{Au}$[a] (nm) | Reaction rate (μmol $s^{-1}$ g(Au)$^{-1}$)[b] | $E_a$ (KJ $mol^{-1}$)[b] | TOF × $10^{-3}$ ($s^{-1}$)[b] |
|---|---|---|---|---|
| Dry gas | 3.5 | 0.21 | 172.1 | 0.14 |
| 25% | 3.5 | 7.55 | 56.95 | 5.21 |
| 50% | 3.5 | 10.78 | 51.79 | 7.43 |
| 75% | 3.5 | 9.70 | 55.84 | 6.69 |

[a] Average gold particle size estimated by statistic analysis from TEM results.
[b] Reaction condition: 80 ppm HCHO/21%$O_2$/$N_2$, RH = 50% (25 °C). $T$ = 25 °C, GHSV = 68,200 $h^{-1}$.

further oxidation of the reactive intermediates of the formates into $CO_2$ and $H_2O$ being rate limiting. It is clear that the presence of moisture not only enhances the formation of the formate intermediates, but also promotes the consumption of the formates. Indeed, $H_2O$ was found to play a key role in the complete oxidation of the formates as clearly shown by DRIFTs data (Fig. 9B). As shown in the inset, it is obvious that the tendency of $CO_2$ variation exactly coincides with the formate consumption as shown in Fig. 9B. This implies that the presence of water could promote the formates' oxidization into $CO_2$. It can be postulated that the introduction of water generates surface hydroxyl groups [Eq. (3)], which were highly active toward $[HCOO]_s$ [Eq. (4)], providing another pathway for complete oxidation of the formates:

$$[O]_s + [H_2O]_s \rightarrow 2[OH]_s \quad (3)$$

$$[HCOO]_s + [OH]_s \rightarrow CO_2(g) + H_2O(g) \quad (4)$$

## 5. Conclusion

It was found that $Au/FeO_x$ prepared by co-precipitation showed superior catalytic activity for the oxidation of HCHO in humid air at room temperature. Both the catalyst calcination temperature and the presence of moisture exerted significant effects on the catalyst performance. $Au/FeO_x$ calcined at 200 °C presented an amorphous phase with a high concentration of hydroxyl groups on its surface. $H_2$-TPR and XPS results revealed that the interaction between Au and $FeO_x$ was stronger in the $Au/FeO_x$-C200 catalyst than $Au/FeO_x$ calcined at higher temperatures. This interaction resulted in increased amounts of active surface oxygen and hydroxyl species, which were reduced by $H_2$ at relatively low temperatures. As a consequence of these characteristics, $Au/FeO_x$-C200 catalyst was found to be highly active for HCHO oxidation at room temperature and under humid air. A certain amount of water was found to be essential for complete oxidation of HCHO at room temperature, although high water concentrations inhibited the catalyst activity, presumably by occupying the active centers. *In situ* DRIFTs studies suggested that the presence of moisture promotes the conversion of the intermediates (such as formates) into $CO_2$ and $H_2O$, which was found to be the rate limiting step for HCHO oxidation. Our results show reducible $FeO_x$-supported Au to be one of most active catalysts for indoor HCHO removal at room temperature and in humid air.

## Conflict of interest

We have no conflict of interest.

## Acknowledgments

The work was supported by the National Natural Foundation of China (Nos. 21073024 and 21373037), Natural Science Foundation of Liaoning Province (No. 201102034) and by the Program for New Century Excellent Talents in University (NCET-07-0136), as well as by the Fundamental Research Funds for the Central Universities (No. DUT12LK23).

## Appendix A. Supplementary data

Supplementary data associated with this article can be found, in the online version, at http://dx.doi.org/10.1016/j.apcatb.2014.02.009.

## References

[1] M. Haruta, N. Yamada, T. Kobayashi, S. Iijima, J. Catal. 115 (1989) 301–309.
[2] M. FlytzaniStephanopoulos, M.B. Boucher, S. Goergen, N. Yi, Phys. Chem. Chem. Phys. 13 (2011) 2517–2527.
[3] O.H. Laguna, F.R. Sarria, M.A. Centeno, J.A. Odriozola, J. Catal. 276 (2010) 360–370.
[4] L. Delannoy, K. Fajerwerg, P. Lakshmanan, C. Potvin, C. Methivier, C. Louis, Appl. Catal. B 94 (2010) 117–124.
[5] B. Liu, Y. Liu, C. Li, W. Hu, P. Jing, Q. Wang, J. Zhang, Appl. Catal. B 127 (2012) 47–58.
[6] H.F. Li, N. Zhang, P. Chen, M.F. Luo, J.Q. Lu, Appl. Catal. B 110 (2011) 279–285.
[7] B.Q. Xu, Y.C. Hong, K.Q. Sun, K.H. Han, G. Liu, Catal. Today 158 (2010) 415–422.
[8] H.Y. Zhu, Y.B. Zhang, Y.N. Shen, X.Z. Yang, S.S. Sheng, T. Wang, M.F. Adebajo, J. Mol. Catal. A Chem. 316 (2010) 100–105.
[9] J. Zhang, Y. Jin, C.Y. Li, Y.N. Shen, L. Han, Z.X. Hu, X.W. Di, Z.L. Liu, Appl. Catal. B 91 (2009) 11–20.
[10] Z.P. Hao, C.Y. Ma, D.H. Wang, W.J. Xue, B.J. Dou, H.L. Wang, Environ. Sci. Technol. 45 (2011) 3628–3634.
[11] B.B. Chen, C. Shi, M. Crocker, Y. Wang, A.M. Zhu, Appl. Catal. B 132–133 (2013) 245–255.
[12] B. Qiao, A. Wang, X. Yang, L.F. Allard, Z. Jiang, Y. Cui, J. Liu, J. Li, T. Zhang, Nat. Chem. 3 (2011) 634–641.
[13] H. Xu, Q. Fu, Y. Yao, X. Bao, Energy Environ. Sci. 5 (2012) 6313.
[14] D. Andreeva, T. Tabakova, V. Idakiev, P. Christov, R. Giovanoli, Appl. Catal. A 169 (1998) 9–14.
[15] C. Milone, R. Ingoglia, L. Schipilliti, C. Crisafulli, G. Neri, S. Galvagno, J. Catal. 236 (2005) 80–90.
[16] H.Y. Zhu, C.Y. Li, Y.N. Shen, M. Jia, S.S. Sheng, M.O. Adebajo, Catal. Commun. 9 (2008) 355–361.
[17] B. Qiao, Y. Deng, Chem. Commun. 17 (2003) 2192–2193.
[18] Y. Wang, A. Zhu, B. Chen, M. Crocker, C. Shi, Catal. Commun. 36 (2013) 52–57.
[19] D.Z. Zhao, C. Shi, X.S. Li, A.M. Zhu, B.W.L. Jang, J. Hazard. Mater. 239 (2012) 362–369.
[20] B. Qiao, A. Wang, J. Lin, L. Li, D. Su, T. Zhang, Appl. Catal. B 105 (2011) 103–110.
[21] G.J. Hutchings, M.S. Hall, A.F. Carley, P. Landon, B.E. Solsona, C.J. Kiely, A. Herzing, M. Makkee, J.A. Moulijn, A. Overweg, J.C. Fierro-Gonzalez, J. Guzman, B.C. Gates, J. Catal. 242 (2006) 71–81.
[22] S.T. Daniells, A.R. Overweg, M. Makkee, J.A. Moulijn, J. Catal. 230 (2005) 52–65.
[23] L. Li, A. Wang, B. Qiao, J. Lin, Y. Huang, X. Wang, T. Zhang, J. Catal. 299 (2013) 90–100.
[24] B. Qiao, J. Zhang, L. Liu, Y. Deng, Appl. Catal. A 340 (2008) 220–228.
[25] S.A.C. Carabineiro, N. Bogdanchikova, P.B. Tavares, J.L. Figueiredo, RSC Adv. 2 (2012) 2957–2965.
[26] D. Andreeva, Gold Bull. 35 (2002) 82–88.
[27] L.I. Ilieva, D.H. Andreeva, A.A. Andreev, Thermochim. Acta 292 (1997) 169–174.
[28] J. Mizera, N. Spiridis, R. Socha, R. Grabowski, K. Samson, J. Korecki, B. Grzybowska, J. Gurgul, L. Kepinski, M.A. Malecka, Catal. Today 187 (2012) 20–29.
[29] C.Y. Li, Y.N. Shen, R.S. Hu, P.P. Li, J. Zhang, Trans. Nonferrous Met. Soc. China 17 (2007) s1107–s1111.
[30] G. Busca, J. Lamotte, J.C. Lavalley, V. Lorenzelli, J. Am. Chem. Soc. 109 (1987) 5197–5202.
[31] G. Šmit, S. Zrnčević, K. Lázár, J. Mol. Catal. A Chem 252 (2006) 103–106.
[32] C. Li, K. Domen, K. Maruya, T. Onishi, J. Catal. 125 (1990) 445–455.
[33] Z. Zhong, J. Highfield, M. Lin, J. Teo, Y.F. Han, Langmuir 24 (2008) 8576–8582.
[34] M.J. Jia, N.H. An, Q.S. Yu, G. Liu, S.Y. Li, W.X. Zhang, J. Hazard. Mater. 186 (2011) 1392–1397.
[35] A.S. Hashmi, G.J. Hutchings, Angew. Chem. Int. Ed. 45 (2006) 7896–7936.
[36] S. Minico, S. Scire, C. Crisafulli, S. Galvagno, Appl. Catal. B 34 (2001) 277–285.